RSC Advances

Volume 1 | Number 1 | Jan 2013 | Pages 1–100

RSC Advances

www.rsc.org/advances

ROYAL SOCIETY OF CHEMISTRY

ROYAL SOCIETY OF CHEMISTRY

www.rsc.org/advances

Journal Name

RSCPublishing

ARTICLE

Facile synthesis of Co_3O_4 with different morphology and their application in supercapacitors

Tian Ouyang, Kui Cheng*, Shuying Kong, Ke Ye, Yinyi Gao, Dingfu Zhang, Guiling Wang, Dianxue Cao *

In this article, Co_3O_4 with different morphologies direct growth on nickel foam is successfully synthesized via a simple hydrothermal method by changing the volume ratio between ethanol and water. The morphology and structure of the as-prepared samples are examined by Scanning electron microscopy, Transmission electron microscopy, X-ray diffractometer and Fourier transform infrared spectroscopy. The electrochemical performances of the Co_3O_4 electrodes are investigated as pseudocapacitor material by cyclic voltammetry and galvanostatic charge/discharge test in 3 mol L^{-1} KOH solution. Results show that the solvent composition plays an important role not only in the morphology but also in the capacitance. Co_3O_4 with a honeycomb structure obtained from the volume ratio of $C_2H_5OH/H_2O=1$ exhibits the highest capacitive performance, 2509.4 F g^{-1} at 1 A g^{-1} and 1754 F g^{-1} at 10 A g^{-1}, which is much larger than that prepared in the pure water and pure ethanol solvent. The electrode also has a satisfactory cycling performance with capacity retention of 74 % after 1000 cycles at 10 A g^{-1}. The enhanced electrochemical performances are ascribed to the honeycomb nanostructure allowing facile electrolyte to flow which fastens electrochemical reaction kinetics. These findings may open up the opportunity on optimizing the hydrothermal synthesis conditions to control the morphology and performance of the products.

Introduction

Electrochemical capacitors, also known as supercapacitors or ultracapacitors, have drawn an increasing attention as the most promising candidates for next-generation energy storage devices due to their high power densities, fast charge-discharge processes, long cycling life, and safe operation[1, 2]. According to the different energy storage mechanisms, electrochemical supercapacitors are divided into two types. One is electrical double-layer capacitors (EDLCs) based on carbonaceous materials which store/deliver energy by non-faradaic surface interactions, leading to higher power density and long cycling life but low specific capacitance[3, 4]. The other one is pseudocapacitors based on conducting polymers and transition metal oxides/hydroxide, where charge is stored/delivered via a fast and reversible surface faradic redox reaction[5, 6]. Despite the specific capacitance of pseudocapacitors is several times larger than EDLCs, pseudocapacitive materials still present a compromise between the power performance and reversibility because of the fast faradic reaction leading to a high demand for the electron transport and fast ion transport[7]. Therefore, a lot of research works have been done in the past few years to improve the performance of the electrochemical capacitor electrode.

Among these pseudocapacitive materials, Co_3O_4 is considered to be one of the most attractive materials owing to its lower toxicity, high theoretical specific capacitance (3560 F g^{-1}), good capability retention and efficient redox charge transfer[8-13]. Thus, various morphology of Co_3O_4 has been reported, such as nanoparticles[14], nanosheets[15], nanowires[16], nanotubes[17] and nanoflowers[18] etc. It has been found that Co_3O_4 based pseudocapacitors mainly depends on properties such as surface area, morphology, and specific orientation of different facets. Therefore, the control over the morphology of nanomaterials with well-defined shape and uniform size remains an important goal of modern synthetic chemistry, especially nanomaterials direct growth on conductive substrate. In comparison to the conventional Co_3O_4/carbon/PTFE electrode[18-21], one-dimensional (1D) Co_3O_4 materials grow on current-collecting substrates could enhance the power density (or rate capability) and cycling stability since this structure not only have the ability to increase the contact area between the electrolyte and active material but also provide accessible channels that facilitate mass and charge transport[22-24]. In order to solve this issue, great efforts have been devoted to creating nanostructured materials with large surface area to enhance the kinetics of ion and electron transport and also shorten the diffusion path of ions and electrons[25].

There are several methods used to prepare cobalt oxides with the controlled morphology, however, most reports focus on the use of surfactant or template, which greatly increased the complicated process to remove these foreign substance. As a facile and effective synthesis method, hydrothermal is widely used for the preparation of Co_3O_4 nanomaterials and various structures have been obtained by changing the temperature, reaction time or reagents[8-11]. However, a very few reports have systematically investigated the effects of solvents composition on the morphology and electrochemical performance of Co_3O_4. Therefore, in this work, Co_3O_4 with different morphology has been successfully synthesized through adding different volume ratio ethanol. The obtained Co_3O_4 electrode exhibited a unique

RSC Advances Accepted Manuscript

ARTICLE

3D hierarchical structure, which delivered large specific capacitances and good electrochemical stability at high rates. This work demonstrate that solvents seem to play a crucial role in shaping the morphology of Co_3O_4 crystals, which could be used to effectively control their structural organization and further improve the capacitive performance.

Experimental

Synthetic Methods

The formation process of Ni foam supported Co_3O_4 electrodes were based on a hydrothermal methods followed by an annealing process. The experimental detail was as follows: The Ni foam was pretreated by degreasing with acetone, etching with 6.0 mol L^{-1} HCl for 15 min, rinsing with water, prior to use. In a typical procedure, 4 mmol $Co(NO)_3$ and 10 mmol $CO(NH_2)_2$ were added to 24 mL C_2H_5OH/H_2O mixed solvent in a volume ratio of 1:0, 1:1 and 0:1 with vigorous stirring. After stirring for 15 min, the mixture was then transferred into a 30 mL Teflon-lined stainless steel autoclave. Afterwards, a piece of Ni foam was put into the autoclave and immersed in the solution. The autoclave was heated gradually to 90 °C and maintained at this temperature for 10 h to allow the growth of Co_3O_4. After that, the autoclave was cooled down to room temperature naturally, then the Ni foam was removed from the growth solution and rinsed with distilled water several times before drying at 60 °C in an oven. Finally, the as-prepared samples were converted to Co_3O_4 via thermal decomposition at 300 °C for 3 h in air.

Materials Characterization

The electrode morphology was examined by a scanning electron Microscope (SEM, JEOL JSM-6480) and a transmission electron microscope (TEM, FEI Teccai G2S-Twin, Philips). The structure was analyzed using an X-ray diffractometer (Rigaku TTR III) with Cu Kα radiation. Chemical bonding information on metal-oxygen and precursor was investigated with Fourier transform infrared spectroscopy (FTIR, Equinos55, Bruker) using the potassium bromide pellet technique.

Electrochemical measurements

The electrochemical measurements were carried out in a three-electrode electrochemical cell containing 3 mol L^{-1} KOH aqueous solution as the electrolyte, the prepared electrode as the working electrode, a saturated calomel electrode (SCE) as reference electrode and a Pt foil as counter-electrode. The cyclic voltammetry (CV) studies were performed on an electrochemical workstation (VMP3, BioLogic, France). Galvanostatic charge-discharge test was conducted using computer controlled cycling equipment (LAND, Wuhan China). All solutions were made with analytical grade chemical reagents and Milli-Q water (18 MΩ cm).

Results and discussion

By using different solvents composition, three samples with different morphologies were obtained. In order to distinguish with each other, the samples prepared using C_2H_5OH/H_2O volume ratios of 1:0, 1:1 and 0:1 were denoted as E-Co_3O_4, EW-Co_3O_4 and W-Co_3O_4, respectively. Their morphologies were detailed characterized by SEM and TEM. Figure 1 shows the SEM images of as-prepared Co_3O_4 samples before and after calcined. It can be seen that all the three samples exhibit relatively uniform, well-dispersed morphology and have its own characteristic, completely different with each other. It can be clearly seen from Figure S1 that Ni foam substrate was completely covered by Co_3O_4. Ni foam as the substrate for the direct growth of Co_3O_4 has many advantages, since that a 3D network structure with micro open cages and zigzag flow

channels. As it shown in Figure 1a and b, E-Co_3O_4 sample exhibits the sheet-like structure. The nanosheets interconnected with each other, creating loose porous nano-structures with abundant open space and electro-active surface sites, however, after calcined, the nanosheets have melted and bonded together,
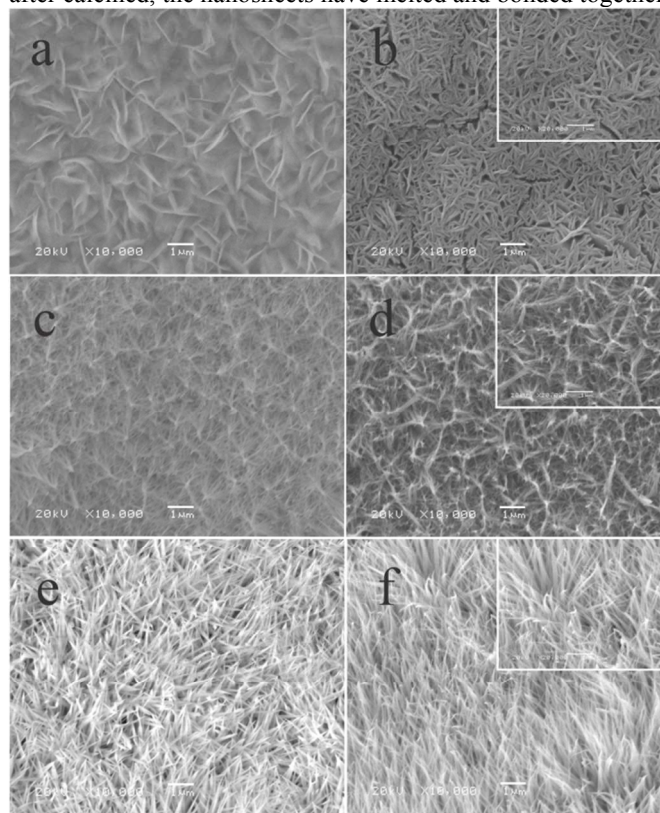

Figure 1 SEM images of E-Co_3O_4 before (a) and after (b) calcined, EW-Co_3O_4 before (c) and after (d) calcined, and W-Co_3O_4 before (e) and after (f) calcined. Insert is the high-magnified SEM images of the as-prepared samples after calcined.

and cracks appeared on the surface. According to Figure 1c and d, the morphology of EW-Co_3O_4 sample remained no obvious changes before and after calcination, which shows a honeycomb-like structure consists of dense nanowires and nanosheets attached to each other. For the sample prepared in pure deionized water (W-Co_3O_4), only nanowire structure was grown on the Ni foam (Figure 1e and f).

The TEM images of the as-prepared Co_3O_4 samples before and after calcined are demonstrated in Figure 2, which provide an insight of individual structures. The TEM images of E-Co_3O_4 (Figure 2a) and W-Co_3O_4 (Figure 2c) samples confirm its assembly as a sheet-like structure and only nanowire-like, respectively. While for the sample EW-Co_3O_4 (Figure 1c), it can be clearly observed that the sample is composed of nanowire and nanosheet. However, all the three Co_3O_4 samples have an obvious change in the morphology that previously solid structure acquired after hydrothermal were converted to a porous structure composed of interconnected nanoparticles with about 20 nm in diameter after calcination. Those porous structures could enhance the accessible channels with the electro-active species, further facilitating mass and charge transport.

Figure 3 shows the XRD patterns of as-prepared Co_3O_4 samples before (a) and after (b) annealing, respectively, and the standard date of spinel-phased Co_3O_4 crystal (JCPDS NO. 43-
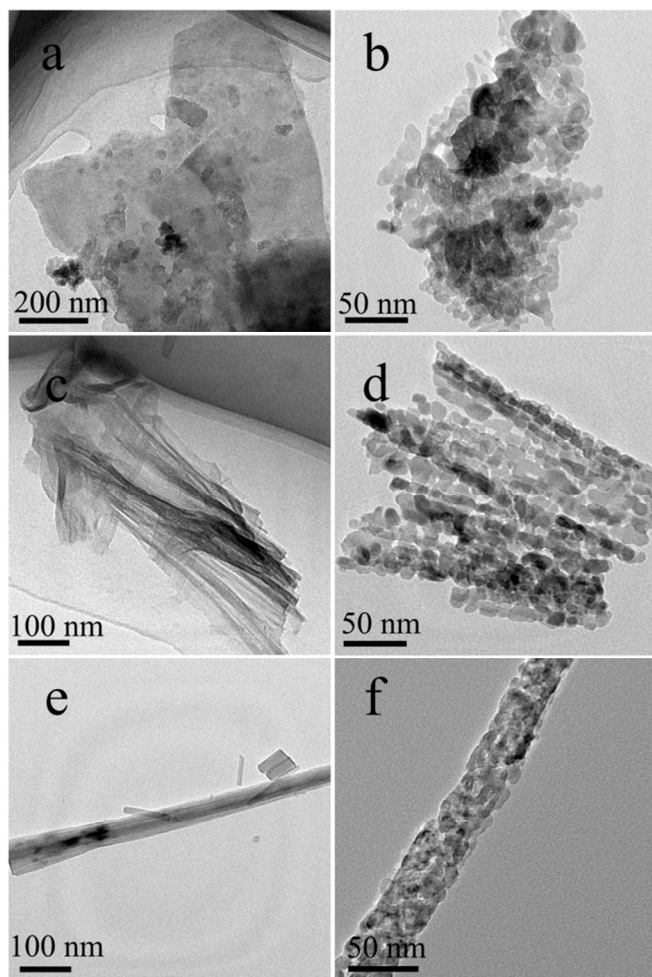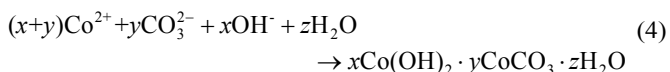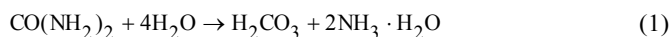
Figure 2 TEM images of E-Co$_3$O$_4$ before (a) and after (b) calcined, EW-Co$_3$O$_4$ before (c) and after (d) calcined, and W-Co$_3$O$_4$ before (e) and after (f) calcined.

1003) is also shown in Figure 3b for comparison. To avoid the effect of Ni foam, all the samples were examined by the powders scratched from nickel foam. As shown, all the samples before the annealing are different and weak crystal. The peak of W-Co$_3$O$_4$ could be assigned to the Co(CO$_3$)0.5(OH)0.11H$_2$O (JCPDS NO. 48-0083), which is agree with the literature reported and the major reactions occurred is as followed[26, 27]:

$$CO(NH_2)_2 + 4H_2O \rightarrow H_2CO_3 + 2NH_3 \cdot H_2O \qquad (1)$$

$$NH_3 \cdot H_2O \rightarrow NH_4^+ + OH^- \qquad (2)$$

$$H_2CO_3 \rightarrow 2H^+ + CO_3^{2-} \qquad (3)$$

$$(x+y)Co^{2+} + yCO_3^{2-} + xOH^- + zH_2O \qquad (4)$$
$$\rightarrow xCo(OH)_2 \cdot yCoCO_3 \cdot zH_2O$$

However, when the ethanol was used as solvent, for the sample E-Co$_3$O$_4$, the peak appeared at 12.8° could be assigned to Co(OOCCH$_3$)$_2$·4H$_2$O (JCPDS NO. 29-0465), indicating that ethanol began to be oxidized during the process of hydrothermal, further reacted with Co^{2+}. The possible reaction is as followed:

$$CH_3CH_2OH + O_2 \rightarrow CH_3COOH + H_2O \qquad (5)$$

$$2CH_3COOH + Co^{2+} \rightarrow (CH_3COO)_2Co + 2H^+ \qquad (6)$$
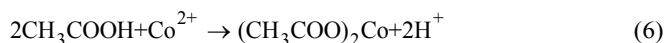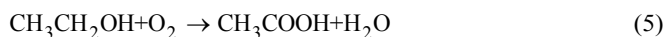
Thus, the precursor of EW-Co$_3$O$_4$ was a mixture of Co(OOCCH$_3$)$_2$·4H$_2$O and Co(CO$_3$)0.5(OH)0.11H$_2$O. After heat treatment, the peaks appeared at 2θ=19.0°, 31.3°, 36.8°, 44.8°, 49.1°, 55.7°, 59.4°, 65.2° and 77.3° can be successfully indexed to (111), (220), (311), (222), (400), (331), (511), (440) and (533) plane reflections of the spinel Co$_3$O$_4$ phase (JCPDS NO. 43-1003), implying that the crystal-line Co$_3$O$_4$ has been formed after annealing treatment (Figure 3b).
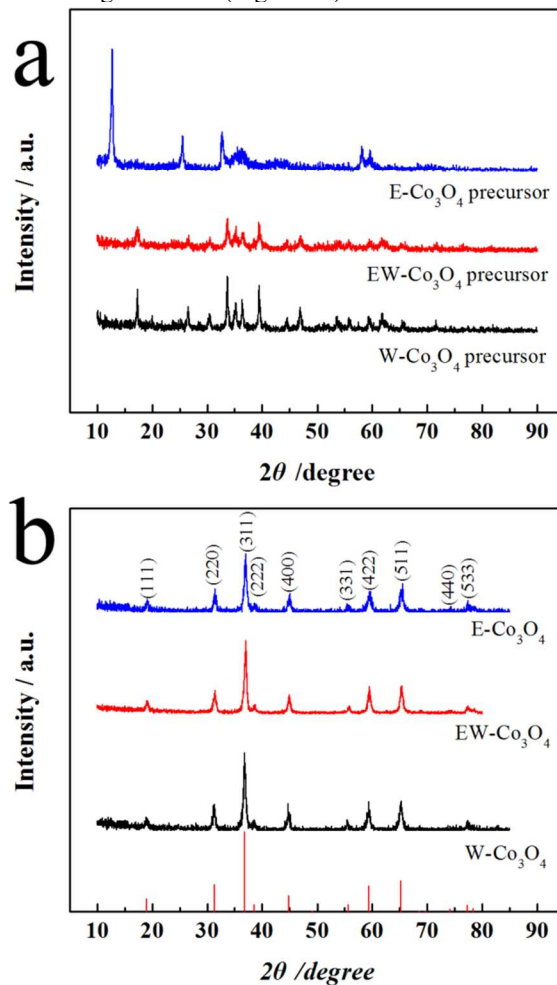

Figure 3 XRD patterns of as-prepared E-Co$_3$O$_4$, EW-Co$_3$O$_4$ and W-Co$_3$O$_4$ before (a) and after (b) annealing at 300 °C for 3 h in air, respectively.

Figure 4a shows the FTIR spectra of the precursor of the three samples. As can been seen, the 1630 and 1384 cm^{-1} bands appeared in both E-Co$_3$O$_4$ and EW-Co$_3$O$_4$ are the characteristic stretching vibration of the –COO– stretching vibration. However, as the CH$_3$CH$_2$OH ratio decreased, the relative strength of –C=O is decreased, revealing that the amount of –COOH is decreased in the precursor of EW-Co$_3$O$_4$. The peaks at 1630 and 1384 cm^{-1} are due to the mode of the –COO– stretching vibration[28]. The EW-Co$_3$O$_4$ and W-Co$_3$O$_4$ precursor film contain stretching vibrations of vOCO$_2$(1499 cm^{-1}) and vCO$_3$$^{-2}$(1384 cm^{-1}, 830 cm^{-1} and 746 cm^{-1})[29, 30] as well as vibration bands of vCo–O (517 cm^{-1}) and vCo–OH (960 cm^{-1})[31]. After annealing treatment, the bands of the precursor film disappeared and two very strong peaks centered at 661 and 565 cm^{-1}characteristic of spinel Co$_3$O$_4$ are noticed, which are consistent with the XRD result. Combined the result of XRD, SEM, TEM and FTIR, it can be found that the solvent

ARTICLE

influences not only the morphology but also the composition of precursor.

In order to demonstrate the excellent electrochemical properties of the as-prepared Co_3O_4 electrode, we scientifically evaluated its supercapacitance behavior through CV and galvanostatic charge-discharge in 3.0 mol L^{-1} KOH aqueous electrolyte using the conventional three-electrode configuration
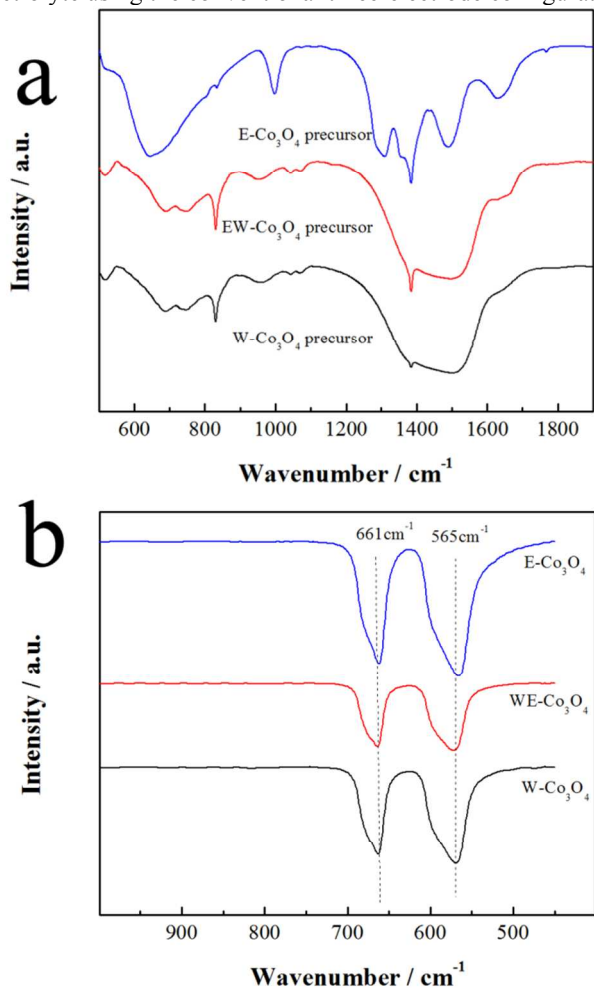

Figure 4 FT-IR spectra of as-prepared $E-Co_3O_4$, $EW-Co_3O_4$ and $W-Co_3O_4$ before (a) and after (b) annealing, respectively.

with a Pt plate counter electrode and a SCE reference electrode. Figure 5 shows the typical CVs of $E-Co_3O_4$ (a), $EW-Co_3O_4$ (b) and $W-Co_3O_4$ (c) in 3.0 mol L^{-1} KOH solution with various sweep rates, respectively. The CV curves of the three Co_3O_4 with different morphology show two oxidation/reduction peaks in the potential range of -0.5 to 0.65 V. The peaks can be respectively attributed to the transition of the redox couple Co(II)/Co(III) and Co(III)/Co(IV)[32], revealing their pseudo-capacitive characteristics. With the increase of the scan rate, the redox current density increased and the anodic and cathodic peaks shifted toward higher and lower potentials, respectively, indicating the quasi-reversible feature of the redox couples. Figure 5d shows the comparison CVs of the as-prepared Co_3O_4 samples with the nickel foam after the solvothermal process at a scan rate of 10 mV s^{-1} in 3.0 mol L^{-1} KOH solution. It can been seen from the insert of Figure 5d that Ni foam only showed a pair of redox peaks which is corresponding to the interconversion between Ni(II) and Ni(III)[33]. However, compared with the as-prepared Co_3O_4 samples, the specific

capacitance of nickel foam can be ignored which the peak currents reached less than 2 mA cm^{-2}. Clearly seen that the CV area of $EW-Co_3O_4$ sample is the largest among the three samples, declares the most ideal capacitive behavior.

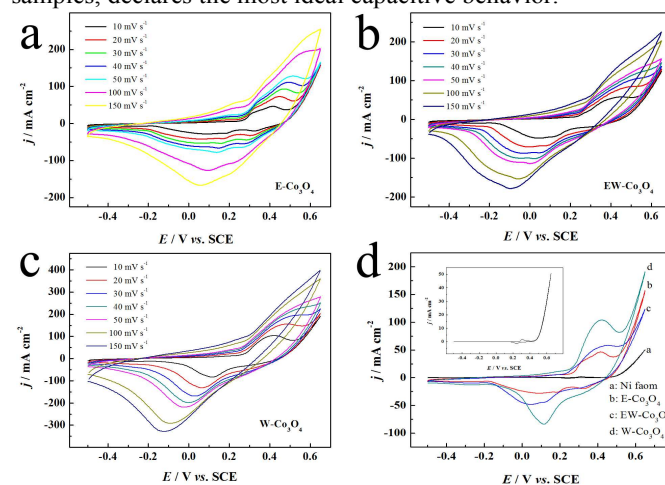**Figure 5** Cyclic voltammograms of $E-Co_3O_4$ (a), $EW-Co_3O_4$ (b) and $W-Co_3O_4$ (c) in 3.0 mol L^{-1} KOH solution at different scan rates, respectively. (d) The Cyclic voltammograms comparision of $E-Co_3O_4$, $EW-Co_3O_4$ $W-Co_3O_4$ and Ni foam after the solvothermal process in 3.0 mol L^{-1} KOH at a 10 mV s^{-1} scan rate.

Figure 6 shows the discharge curves of $E-Co_3O_4$ (a), $EW-Co_3O_4$ (b) and $W-Co_3O_4$ (c) in 3.0 mol L^{-1} KOH solution at different current densities. The specific capacitances were calculated according to the following equation:

$$C_m = (i \times \Delta t) / (\Delta V \times m) \tag{7}$$

where C_m (F g^{-1}) is the specific capacitance, i (A) is the discharge current, Δt (s) is the discharge time, ΔV (V) is the

Figure 6 The discharge curves of $E-Co_3O_4$ (a), $EW-Co_3O_4$ (b) and $W-Co_3O_4$ (c) in 3.0 mol L^{-1} KOH solution at different current densities. (d) Plots of specific capacitance per gram and per area versus current density for the as-prepared Co_3O_4 samples.

voltage window for discharge, and m (g) is the total mass of active material in the electrode. The specific capacitance per gram and per area versus current density for the as-prepared Co_3O_4 samples is shown in Figure 6d. The mass loadings of $E-Co_3O_4$, $EW-Co_3O_4$ and $W-Co_3O_4$ (in mg of electrochemically active material per cm^2 of nickel foam) are 3.8, 2.1 and 3 mg

cm^{-2}, respectively. As shown in the result, EW-Co$_3$O$_4$ sample displays an extremely performance for supercapacitors during the three samples and the specific capacitance values were measured to be 2509.4, 2004.2, 1754.9, 1221.6, 342.8 F g^{-1} (5.26, 4.21, 3.69, 2.57 and 0.72 F cm^{-2}) at the current density of 1, 5, 10, 20, and 50 A g^{-1}, respectively. It was also found that the capacitance decreased with an increase in discharge current density, which was caused by the electrode resistance and the relatively low utilization of the active material under higher discharge current densities.

In order to better evaluation the electrochemical properties of the as-prepared Co$_3$O$_4$ materials, we prepared the electrode using the conventional Co$_3$O$_4$/carbon/PTFE technology. Typically, 85 wt.% Co$_3$O$_4$ powder (scratched from nickel foam), 10 wt.% acetylene black as a conducting agent and 5 wt.% polytetrafluorethylene (PTFE) as a binder were homogeneously mixed and pressed into a nickel foam (1 cm*1 cm) current collector under a pressure of 8 MPa. The mass loading of each electrode is about 6 mg cm^{-2}. Their supercapacitance behaviors were tested through CV and galvanostatic charge-discharge methods in 3.0 mol L^{-1} KOH aqueous electrolyte using the conventional three-electrode. The results are shown in Figure S2, S3 and S4. Cleary, the electrochemical performance of the three samples is far below that of direct growth on the Ni foam, which may cause by these nanostructures, can improve the contact between electroactive materials and current collectors which facilitates better kinetics. However, among these three samples, EW-Co$_3$O$_4$ sample shows the highest performance,

which is caused by EW-Co$_3$O$_4$ sample have a large specific surface area, further will benefit for enhancing the kinetics of ion and electron transport.

Cycling stability or cycling life is an important requirement for the as-prepared electrode materials in the practical supercapacitor applications. The cyclic performance of the EW-Co$_3$O$_4$ sample examined by galvanostatic charge-discharge tests at a current density of 10 A g^{-1} for 1000 cycles is depicted in Figure 7. The columbic efficiency is also shown in Figure 7, which was calculated based on the following equation:

$$\eta = t_d / t_c \times 100 \tag{8}$$

In this equation, t_c and t_d represent the time of charge and discharge, respectively. It is apparent that the specific capacitance decreased obviously in the first 200 with cycles. In order to explain the initial capacitance decay, EIS analysis is performed and the result is displayed in the insert of Figure 7. All the impedance spectra were composed of one semicircle component at high-frequency followed by a linear component at the low-frequency. Obviously, the EW-Co$_3$O$_4$ electrode before cycles exhibits lower transfer resistance and closer straight line to 90°, demonstrating the lower diffusion resistance of ions and improved electrolyte ions diffusion[34]. After 1000 cycles, the specific capacitance remains 1225.7 F g^{-1} with capacitance retention of 74%. The columbic efficiency remains above 99% within 1000 cycles.

Table 1. Comparison of the specific capacity at different current densities for recently reported Co$_3$O$_4$ materials

Current Density A g^{-1}	1	2	5	10	20	Cycle	Method	Electrode	Reference
Co$_3$O$_4$ nanowire array	-	323 [a]	-	290	272	Not given	Hydrothermal	Grown on Ni foam	[31]
hollow Co$_3$O$_4$ nanowire	-	295	-	271	258	82% returned after 7500 cycles at 10 A g^{-1}	Hydrothermal	Grown on Ni foam	[35]
Co$_3$O$_4$/C flower-like nanostructures	290.9	255.3	-	-	-	Not given	Solvothermal	Powder + acetylene black+ PTFE	[18]
Co$_3$O$_4$ /rGO/CNTs Hybrid	-	364	330	-	-	Not given	Hydrothermal	Grown on rGO/CNTs Hybrid Paper	[36]
porous Co$_3$O$_4$ nanoflake array	369	351	-	264	242	97.4% returned after 4000 cycles at 2 A g^{-1}	Hydrothermal	Grown on Ni foam	[15]
Co$_3$O$_4$ -CNFs	552	524	-	-	-	99% returned after 2000 cycles at 4 A g^{-1}	Electrospinning	Powder + acetylene black+ PVDF	[37]
Co$_3$O$_4$ hollow microspheres	-	394.4	386	360	319	92% returned after 500 cycles at 2 A g^{-1}	annealing	Powder + acetylene black+ PVDF	[19]
brush-like Co$_3$O$_4$ nanowires	1525	-	-	-	-	94% returned after 5000 cycles at 1 A g^{-1}	Solvothermal	Grown on carbon fiber paper	[38]
Co$_3$O$_4$ nanofibers	340	-	315	296	-	94% returned after 1000 cycles at 1 A g^{-1}	electrospinning	Powder + acetylene black+ PVDF	[21]
Reduced Co$_3$O$_4$ NWs	-	978	770	484	-	90% returned after 2000 cycles at 2 A g^{-1}	solution reduction	Grown on Ni foam	[39]
EW- Co$_3$O$_4$	2509	-	2004	1754	1221	74% returned after 1000 cycles at 10 A g^{-1}	Solvothermal	Grown on Ni foam	This work

[a] specific capacitance per gram

As presented in Table 1, we have summarized the rate performance of recently reported Co$_3$O$_4$ based materials with our

EW-Co$_3$O$_4$ electrode. Clearly, this is a rather high value compared to literature results (Table 1)[15, 18, 19, 21, 31, 35-39]. The

enhanced performance of the EW-Co₃O₄ electrode can be ascribed to the follow reasons: (1) The electro-active materials were directly grown onto nickel foam without any conducting additive and binder, therefore, the utilization of the active material is high. (2) The EW-Co₃O₄ sample provided a large specific surface area with many holes, benefitting from enhancing the kinetics of ion and electron transport and also shortening the diffusion path of ions and electrons.

Conclusions

In summary, Co_3O_4 nanostructure with different morphologies has been easily obtained through a simple hydrothermal method with changing the solvents composition. The electrochemical performance of the as-prepared Co_3O_4 samples has been done without adding any binder or carbon additive. The specific capacitance of EW-Co_3O_4 electrode prepared in C_2H_5OH/H_2O volume ratios 1/1 is 2509.4 $F \cdot g^{-1}$ at 1 A g^{-1} and 1754 $F \cdot g^{-1}$ at 10 A g^{-1}, which is much larger than that on the Co_3O_4 nanowire arrays prepared in the pure water and pure ethanol solvent, as well as a rather high value compared to literature results. The enhanced performance is possibly due to its unique structure that could greatly raise the utilization efficiency of active materials and guarantee a superior property for electrolyte diffusion. The as-prepared honeycomb-like Co_3O_4 electrode has a promising future for electrochemical supercapacitors application.
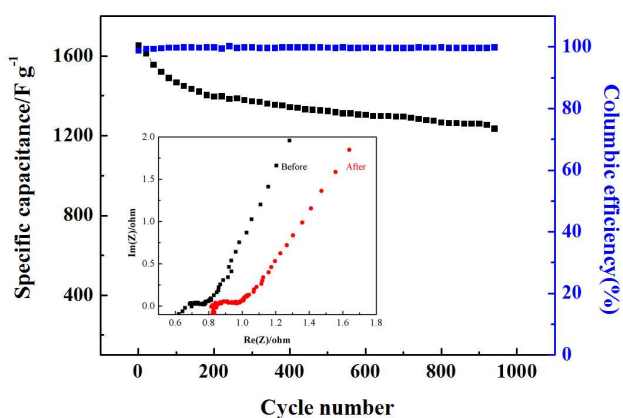

Figure 7. The discharge specific capacitance and the columbic efficiency of EW-Co_3O_4 sample for 1000 cycles at 10 A g^{-1} in 3.0 mol L^{-1} KOH solution. The insert is the EIS date of EW-Co_3O_4 sample before and after 1000 cycles.

Acknowledgements

Notes and references

Key Laboratory of Superlight Material and Surface Technology of Ministry of Education, College of Material Science and Chemical Engineering, Harbin Engineering University, Harbin, 150001, P.R.China. E-mail: chengkui@hrbeu.edu.cn, caodianxue@hrbeu.edu.cn.

† Electronic Supplementary Information (ESI) available: Experimental details and characterizations. See DOI: 10.1039/b000000x/

1. J. R. Miller, R. Outlaw and B. Holloway, *Science*, 2010, **329**, 1637-1639.
2. T. Brezesinski, J. Wang, S. H. Tolbert and B. Dunn, *Nature Materials*, 2010, **9**, 146-151.
3. L. Wei and G. Yushin, *Nano Energy*, 2012, **1**, 552-565.
4. Q. Wu, Y. Xu, Z. Yao, A. Liu and G. Shi, *Acs Nano*, 2010, **4**, 1963-1970.
5. X.-h. Xia, J.-p. Tu, X.-l. Wang, C.-d. Gu and X.-b. Zhao, *Journal of Materials Chemistry*, 2011, **21**, 671-679.
6. H. Wang, H. S. Casalongue, Y. Liang and H. Dai, *Journal of the American Chemical Society*, 2010, **132**, 7472-7477.
7. B. Conway, V. Birss and J. Wojtowicz, *Journal of Power Sources*, 1997, **66**, 1-14.
8. H. Wang, L. Zhang, X. Tan, C. M. Holt, B. Zahiri, B. C. Olsen and D. Mitlin, *The Journal of Physical Chemistry C*, 2011, **115**, 17599-17605.
9. L. Cui, J. Li and X.-G. Zhang, *Journal of Applied Electrochemistry*, 2009, **39**, 1871-1876.
10. G. Tong, Y. Liu and J. Guan, *Journal of Alloys and Compounds*, 2014, **601**, 167-174.
11. H. Sun, M. Ahmad and J. Zhu, *Electrochimica Acta*, 2013, **89**, 199-205.
12. C. Wu, Q. Shen, R. Mi, S. Deng, Y. Shu, H. Wang, J. Liu and H. Yan, *Journal of Materials Chemistry A*, 2014, **2**, 15987-15994.
13. N. Padmanathan, S. Selladurai and K. M. Razeeb, *Rsc Advances*, 2015, **5**, 12700-12709.
14. C. Yuan, L. Yang, L. Hou, L. Shen, F. Zhang, D. Li and X. Zhang, *Journal of Materials Chemistry*, 2011, **21**, 18183-18185.
15. Y. Q. Zhang, L. Li, S. J. Shi, Q. Q. Xiong, X. Y. Zhao, X. L. Wang, C. D. Gu and J. P. Tu, *Journal of Power Sources*, 2014, **256**, 200-205.
16. B. Vidyadharan, R. A. Aziz, I. I. Misnon, G. M. Anil Kumar, J. Ismail, M. M. Yusoff and R. Jose, *Journal of Power Sources*, 2014, **270**, 526-535.
17. J. Xu, L. Gao, J. Cao, W. Wang and Z. Chen, *Electrochimica Acta*, 2010, **56**, 732-736.
18. J. Jiang, W. Shi, S. Song, Q. Hao, W. Fan, X. Xia, X. Zhang, Q. Wang, C. Liu and D. Yan, *Journal of Power Sources*, 2014, **248**, 1281-1289.
19. Y. Wang, A. Pan, Q. Zhu, Z. Nie, Y. Zhang, Y. Tang, S. Liang and G. Cao, *Journal of Power Sources*, 2014, **272**, 107-112.
20. F. Zhou, Q. Liu, J. Gu, W. Zhang and D. Zhang, *Journal of Power Sources*, 2015, **273**, 945-953.
21. M. Kumar, A. Subramania and K. Balakrishnan, *Electrochimica Acta*, 2014, **149**, 152-158.
22. T. He, D. Chen and X. Jiao, *Chemistry of Materials*, 2004, **16**, 737-743.
23. H. Liang, J. M. Raitano, L. Zhang and S.-W. Chan, *Chemical Communications*, 2009, 7569-7571.
24. L. Yang, S. Cheng, Y. Ding, X. Zhu, Z. L. Wang and M. Liu, *Nano letters*, 2011, **12**, 321-325.

25. X. Zhao, B. M. Sánchez, P. J. Dobson and P. S. Grant, *Nanoscale*, 2011, **3**, 839-855.

26. Y. Wang, H. Xia, L. Lu and J. Lin, *ACS Nano*, 2010, **4**, 1425-1432.

27. J. Jiang, J. P. Liu, X. T. Huang, Y. Y. Li, R. M. Ding, X. X. Ji, Y. Y. Hu, Q. B. Chi and Z. H. Zhu, *Crystal Growth & Design*, 2009, **10**, 70-75.

28. H. Lewandowski, E. Koglin and R. J. Meier, *Vibrational Spectroscopy*, 2005, **39**, 15-22.

29. K. T. Ehlsissen, A. Delahaye-Vidal, P. Genin, M. Figlarz and P. Willmann, *Journal of Materials Chemistry*, 1993, **3**, 883-888.

30. M. Y. Nassar, *Materials Letters*, 2013, **94**, 112-115.

31. X.-h. Xia, J.-p. Tu, Y.-q. Zhang, Y.-j. Mai, X.-l. Wang, C.-d. Gu and X.-b. Zhao, *Rsc Advances*, 2012, **2**, 1835-1841.

32. Y. Gao, S. Chen, D. Cao, G. Wang and J. Yin, *Journal of Power Sources*, 2010, **195**, 1757-1760.

33. K. Cheng, F. Yang, K. Ye, Y. Li, S. Yang, J. Yin, G. Wang and D. Cao, *Journal of Materials Chemistry A*, 2013, **1**, 14246-14252.

34. A. L. M. Reddy, M. M. Shaijumon, S. R. Gowda and P. M. Ajayan, *The Journal of Physical Chemistry C*, 2009, **114**, 658-663.

35. X.-h. Xia, J.-p. Tu, Y.-j. Mai, X.-l. Wang, C.-d. Gu and X.-b. Zhao, *Journal of Materials Chemistry*, 2011, **21**, 9319-9325.

36. C. Yuan, L. Yang, L. Hou, J. Li, Y. Sun, X. Zhang, L. Shen, X. Lu, S. Xiong and X. W. D. Lou, *Advanced Functional Materials*, 2012, **22**, 2560-2566.

37. F. Zhang, C. Yuan, J. Zhu, J. Wang, X. Zhang and X. W. D. Lou, *Advanced Functional Materials*, 2013, **23**, 3909-3915.

38. R. Rakhi, W. Chen, D. Cha and H. Alshareef, *Nano letters*, 2012, **12**, 2559-2567.

39. Y. Wang, T. Zhou, K. Jiang, P. Da, Z. Peng, J. Tang, B. Kong, W. B. Cai, Z. Yang and G. Zheng, *Advanced Energy Materials*, 2014, **4**.